RSNA
Radiological Society
of North America

Radiology

RADIOLOGY.RSNA.ORG
OCTOBER 2010
VOLUME 257 NUMBER 1
RADLAX 257 (1) 1–302

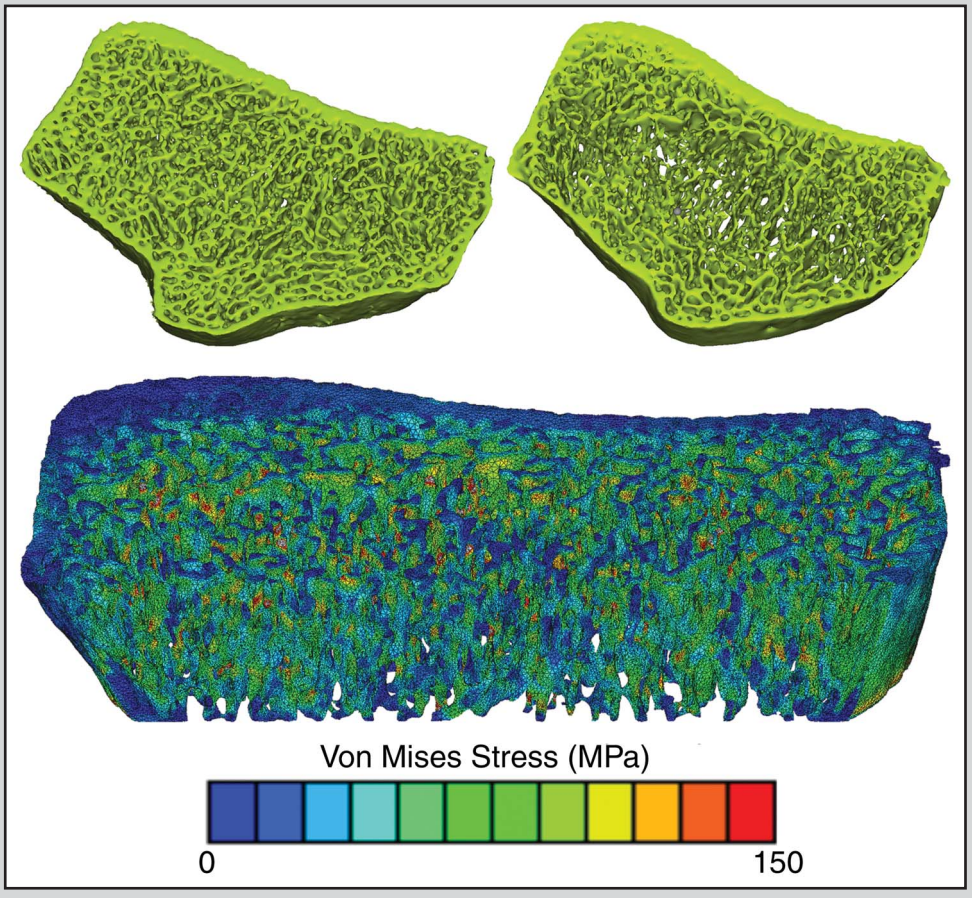

Women with Anorexia Nervosa: Finite Element and Trabecular Structure Analysis by Using Flat-Panel Volume CT[1]

Conor J. Walsh, PhD
Catherine M. Phan, MD
Madhusmita Misra, MD
Miriam A. Bredella, MD
Karen K. Miller, MD
Pouneh K. Fazeli, MD
Harun H. Bayraktar, PhD
Anne Klibanski, MD
Rajiv Gupta, MD, PhD

Purpose: To use finite element modeling based on flat-panel volume computed tomography (CT) and bone mineral density (BMD) provided by dual-energy x-ray absorptiometry (DXA) to compare bone failure load, stiffness, and trabecular structure in women with anorexia nervosa (AN) and age-matched normal-weight control subjects.

Materials and Methods: The study was approved by the institutional review board and complied with HIPAA guidelines. Informed consent was obtained. Fourteen women, eight with AN (mean age, 26.6 years) and six control subjects (mean age, 26.3 years), underwent flat-panel volume CT of the distal radius to determine apparent trabecular bone volume fraction (BV/TV), apparent trabecular number (TbN), apparent trabecular thickness (TbTh), and apparent trabecular separation (TbSp). Bone strength and stiffness were calculated from uniaxial compression tests by using finite element models created from flat-panel volume CT. DXA was used to determine BMD of the radius, lumbar spine, and hip. Means ± standard deviations of all variables were calculated for both groups and compared (Student *t* test). Univariate regression analysis and stepwise regression modeling were performed.

Results: Patients with AN had lower values for stiffness (284.77 kN/mm ± 76.14 vs 389.97 kN/mm ± 84.90, $P = .04$), failure load (4.98 kN ± 1.23 vs 7.01 kN ± 1.52, $P = .02$), BV/TV (0.32% ± 0.09 vs 0.44% ± 0.02, $P = .007$), and TbN (1.15 mm^{-3} ± 0.20 vs 1.43 mm^{-3} ± 0.13, $P = .008$) and higher values for TbSp (0.62 mm ± 0.20 vs 0.40 mm ± 0.04, $P = .02$) compared with normal-weight control subjects. TbTh was lower in women with AN ($P = .1$). BMD measurements were significantly lower for the AN group. BMD measurements and trabecular parameters (except TbTh) correlated with stiffness and failure load ($r = 0.58$ to 0.83).

Conclusion: Failure load and stiffness are abnormal in women with AN compared with those in normal-weight control subjects and correlate with BMD and trabecular parameters.

[1] From the Department of Mechanical Engineering, Massachusetts Institute of Technology, 77 Massachusetts Ave, Room 3-470, Cambridge, MA 02139 (C.J.W.); Department of Radiology (C.M.P., M.A.B., R.G.) and Neuroendocrine Unit, Department of Medicine (M.M., K.K.M., P.K.F., A.K.), Massachusetts General Hospital, Boston, Mass; and Dassault Systèmes Simulia, Providence, RI (H.H.B.). Received January 28, 2010; revision requested March 17; revision received April 23; accepted April 30; final version accepted May 17. **Address correspondence to** C.J.W. (e-mail: *walshcj@alm.mit.edu*).

Anorexia nervosa (AN) is a prevalent eating disorder among women in the United States (1,2) and is associated with substantial bone loss (3,4) and low bone mineral density (BMD) (5). Bone strength is not only determined by BMD but also by the spatial arrangement of the trabeculae and the mechanical properties of bone (6). Trabecular structure parameters have been shown to better distinguish healthy from diseased bone than BMD alone (7,8). However, these measures do not include information about bone mechanical properties or tissue level strain.

Finite element analysis is a method that can be used to evaluate stiffness and strength of bone in vivo. It offers the ability to directly evaluate bone mechanical properties and to predict failure load (7) and fracture risk (8). Finite element models of the distal radius have been created from in vivo three-dimensional peripheral quantitative computed tomographic (CT) images (9–11) and more recently from high-resolution peripheral quantitative CT images (12,13) with spatial resolutions of 165 and 82 μm, respectively. These models have primarily been constructed by segmenting out cortical and trabecular bone from the surrounding tissues with a thresholding technique based on attenuation so that bone trabecular architecture is directly incorporated. By using these models, good correlations have been obtained between predicted stiffness and failure load and those obtained from experiments on cadaveric forearms (9,12).

Despite extensive literature demonstrating low BMD in patients with AN, data regarding bone structural changes are sparse. Flat-panel volume CT has been previously introduced and validated as a noninvasive technique for the evaluation of trabecular bone structure in adolescent girls with AN (8). It is an imaging modality that combines the advances in CT with digital flat-panel detector technology and is capable of high-resolution (150 × 150 × 150 μm) in vivo imaging (13). However, its use for the creation of finite element models of bone trabecular architecture has not yet been examined.

By using finite element modeling based on flat-panel volume CT and BMD provided by dual-energy x-ray absorptiometry (DXA), the purpose of our study was to compare bone failure load, stiffness, and trabecular structure in women with AN and age-matched normal-weight healthy control subjects.

Advances in Knowledge

- Flat-panel volume CT images of the distal radius at 150-μm resolution allow the creation of finite element models that include trabecular architecture.
- Bone failure load and stiffness are reduced for women with anorexia nervosa (AN) compared with normal-weight control subjects.
- Bone mineral density and trabecular structure parameters, apart from trabecular bone thickness, correlate with bone failure load and stiffness.

Implication for Patient Care

- Flat-panel volume CT imaging could potentially be used as a noninvasive technique for estimating bone failure load and stiffness from finite element models in women with AN.

Materials and Methods

Study Design

The study was approved by our institutional review board at Massachusetts General Hospital and complied with Health Insurance Portability and Accountability Act guidelines. Written informed consent was obtained from all subjects. Between June 2008 and December 2008, 14 women aged 20–41 years, including eight women with AN (mean age, 26.6 years; age range, 20–41 years) and six normal-weight healthy control subjects of similar age (mean age, 26.3 years; age range, 20–39 years), were studied. All women with AN fulfilled *Diagnostic and Statistical Manual of Mental Disorders*, fourth edition, criteria for AN (14). Exclusion criteria included pregnancy; diabetes mellitus; thyroid, cardiac, liver, or renal disease; or medications known to affect bone metabolism. The normal weight for healthy control subjects was defined as 90%–100% of ideal body weight for age. In addition, exclusion criteria for healthy control subjects included history of an eating disorder or amenorrhea. All subjects were examined during one study visit at our clinical research center.

Flat-Panel Volume CT Image Acquisition

Flat-panel volume CT (Siemens, Forchheim, Germany) was performed to obtain 150-μm^3 resolution CT images of the nondominant distal radius, unless there was a history of fracture at that site, in which case the nonfractured radius was scanned. Design and use of the flat-panel volume CT scanner has been described previously (8,13). The flat-panel volume CT scanner was utilized in the 1 × 1 binning mode, providing an effective field of view of 25 × 25 × 4.5 cm and the highest resolution of 150 μm achievable with the

Published online before print
10.1148/radiol.10100222

Radiology 2010; 257:167–174

Abbreviations:
AN = anorexia nervosa
BMD = bone mineral density
BV/TV = apparent trabecular bone volume fraction
DXA = dual-energy x-ray absorptiometry
TbN = apparent trabecular number
TbSp = apparent trabecular separation
TbTh = apparent trabecular thickness

Author contributions:
Guarantors of integrity of entire study, C.J.W., C.M.P., M.M., M.A.B., R.G.; study concepts/study design or data acquisition or data analysis/interpretation, all authors; manuscript drafting or manuscript revision for important intellectual content, all authors; manuscript final version approval, all authors; literature research, C.J.W., C.M.P., M.M., M.A.B., H.H.B., A.K.; clinical studies, C.J.W., C.M.P., M.A.B., K.K.M., P.K.F., A.K., R.G.; experimental studies, M.M., H.H.B., A.K., R.G.; statistical analysis, C.J.W., C.M.P., M.M., M.A.B.; and manuscript editing, all authors

Funding:
This work was supported by National Institutes of Health grants (nos. R01 DK052625, M01 RR01066, and ULI RR0257801).

Authors stated no financial relationship to disclose.

scanner. Tube voltage and tube current setting were 100 kV and 30 mA, respectively, which led to a delivered radiation dose of 0.027 mSv. A modified Feldkamp algorithm was used for cone-beam reconstruction (13).

The wrist of the subject was immobilized during the examination by strapping it to a foam cushion. For each case, 100 CT sections were obtained, delivering a three-dimensional representation of approximately 20 mm in the axial direction. All measurements were performed 10 mm proximal from the articular surface, corresponding to the DXA measurement of the ultradistal radius.

Measurement of Trabecular Structure

Trabecular structure parameters were calculated by using software (MicroView; GE Healthcare, Waukesha, Wis). For each distal radius, a three-dimensional oval region of interest was defined within the distal radius to cover a maximum area of trabecular bone without including any cortical bone. The observer (C.M.P., 8 years of experience in radiology) was blinded to patient status (patient with AN vs control subject). Trabecular bone was segmented from marrow, with the individual threshold level defined by the automatic threshold level function of the software (15–17). The function provides automated segmentation by generating the attenuation histogram of the volume of interest and fitting the data by using the Otsu algorithm (18). By using standard methods from histomorphometry (19), the following measures of trabecular structure were calculated: apparent trabecular bone volume fraction (BV/TV) as a percentage, apparent trabecular number (TbN) in 1/millimeters, apparent trabecular thickness (TbTh) in millimeters, and apparent trabecular separation (TbSp) in millimeters.

BMD and Body Composition

We used DXA (QDR 4500; Hologic, Waltham, Mass) to measure BMD and body composition. BMD (in grams per square centimeter) was assessed at the ultradistal radius, radius, lumbar spine, hip, femoral neck, and total body. T and *z* scores were calculated. We used DXA to obtain measurements of fat mass (in kilograms), lean mass (in kilograms), and percentage of body fat.

Three-dimensional Finite Element Modeling

Each subject was scanned with a calibration phantom to standardize gray-scale values and maintain consistency. This custom-designed calibration phantom consisting of three test tubes embedded within the foam cushion attached to a hand splint was used for stabilizing the wrist joint. The first test tube contained normal saline to provide calibration for 0 HU. The other two test tubes contained calibrated solutions of $Ca^2(HPO_4)^3$ that measured 130 and 200 HU with a conventional multidetector CT (8). Before processing, CT images were supersampled by a factor of two by using bilinear interpolation, and a contrast enhancement filter was applied for better differentiation of the fine trabecular bone from the surrounding tissue. Threshold-based segmentation of the cortical and trabecular structure was performed with software (MIMICS; Materialise, Leuven, Belgium) to obtain 5-mm axial sections of the distal radius. Region growing was applied to the segmented structure to remove any floating portions. Three-dimensional models were created by using a matrix reduction setting of 1 × 1 and the advanced edge triangle reduction method. This model was remeshed by using software (MIMICS) to ensure that the triangular element size, shape, and quality were high and that trabecular plates and rods had at least four elements across them. This surface finite element model was then converted to a three-dimensional solid mesh with linear tetrahedral elements in Abaqus CAE (SIMULIA, Providence, RI), resulting in approximately 2–8 million first-order tetrahedral elements (Fig 1).

Finite Element Analysis

A 0.1% axial strain was prescribed to the top face of the 5-mm section of the distal radius, and axial displacements at the bottom face were constrained, simulating a zero-friction compression test (Fig 2). Equal linear elastic material properties were applied to the cortical and trabecular bone (Young modulus, 17 GPa [20]; Poisson ratio, 0.3). The finite element models were solved by using Abaqus with 32 cores on a Linux cluster with E5462 processors (Intel, Santa Clara, Calif). Each computer node has a total of eight cores and 32 GB of memory. The sum of the reaction forces of the displaced nodes was recorded. The apparent stiffness of each bone segment was calculated by dividing the reaction force by the applied displacement. The element volumes, stresses, and strain energy density were also exported from Abaqus. An effective strain, ε_{eff}, for each element was calculated from the strain energy density, U, and the elastic modulus of the material, E, as follows:

$$\varepsilon_{eff} = \sqrt{\frac{2U}{E}}.$$

The estimated failure load for the bone specimen was computed on the basis of a failure criterion from Pistoia et al (9), where failure was assumed to occur when 2% of the bone tissue was strained beyond a critical limit of 0.7%.

Statistical Analysis

Software (JMP Statistical Database, version 4; SAS Institute, Cary, NC) was used for statistical analysis. Results are reported as means ± standard deviations. A P value less than .05 was considered to indicate a statistically significant difference. Variables were compared by using the Student t test.

Univariate regression analysis was performed to determine associations of mechanical properties (stiffness, failure load) with trabecular structure measurements, BMD, lean mass, and body mass index. Variables were tested for normality of distribution by using the Shapiro-Wilk test. We used Pearson correlation when data were normally distributed and Spearman correlation when data were not normally distributed. Univariate regression analysis was performed to determine the correlation between stiffness and strength.

Figure 1

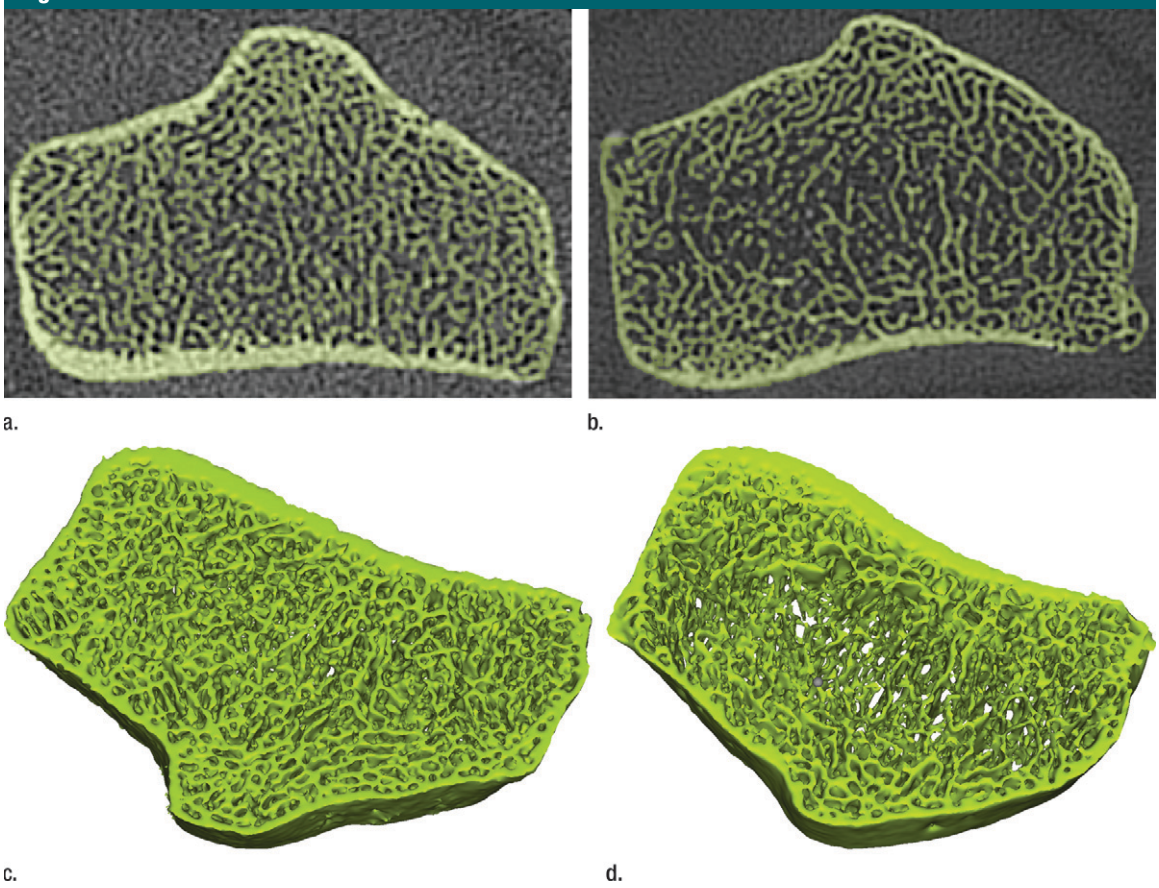

Figure 1: Axial flat-panel volume CT images of distal radius in **(a)** control subject and **(b)** woman with AN. Masks (green) created by segmenting out the cortical and trabecular bone structure with a thresholding technique are overlaid on the flat-panel volume CT images. Corresponding three-dimensional models for **(c)** control subject and **(d)** woman with AN were created with software (MIMICS) by compiling the masks of 5-mm sectional flat-panel volume CT images. Flat-panel volume CT images and three-dimensional models clearly demonstrate rarefaction of trabeculae and thinning of the cortical shell of the distal radius in AN compared with that in control subject.

Stepwise regression modeling was performed to determine predictors of stiffness and failure load for the whole cohort. Potential predictors that were entered into the model included TbN, TbTh, and BV/TV. We did not include TbSp in the model because this was strongly correlated with TbN. We also used stepwise regression to determine whether bone structural parameters remained significant predictors of stiffness and failure load after controlling for body mass index, fat mass, or diagnostic category.

Figure 2

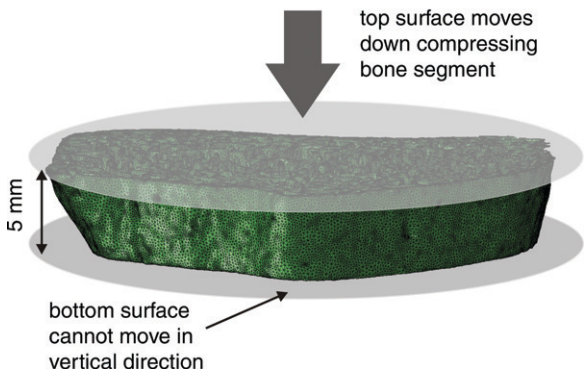

Figure 2: Illustration of the simulated compression test performed with software (Abaqus). The top face (thick arrow) is assigned 0.1% strain, while the bottom face is constrained in the vertical direction.

Results

Clinical characteristics of the cohort are summarized in Table 1. As expected, women with AN had lower body mass index, fat mass, and percentage of body fat than control subjects. The two groups did not differ in age or lean mass.

Trabecular Structure

Trabecular structure parameters (BV/TV, TbN, and TbSp) were significantly

Table 1

Clinical Characteristics of AN and Control Groups

Variable	AN Group ($n = 8$)	Control Group ($n = 6$)	*P* Value
Age (y)	26.6 ± 7.1	26.3 ± 6.9	.94
Body mass index (kg/m^2)	17.4 ± 1.4	24.4 ± 2.5	.0005
Weight (kg)	47.7 ± 7.7	66.3 ± 7.04	.001
Fat mass (kg)	7.6 ± 2.2	21.7 ± 5.3	.001
Lean mass (kg)	38.3 ± 3.2	42.2 ± 4.1	.86
Percentage of body fat	15.9 ± 4.1	32.6 ± 5.7	.0002
Age of onset (y)	19.4 ± 4.4	…	…
Duration of disease (y)	7.2 ± 7.9	…	…
Duration of amenorrhea (mo)	16.2 ± 17.7	…	…

Note.—Data are means ± standard deviations.

Table 2

Trabecular and Mechanical Parameters of AN and Control Groups

Parameter	AN Group ($n = 8$)	Control Group ($n = 6$)	Percentage Difference*	*P* Value
BV/TV (%)	0.32 ± 0.09	0.44 ± 0.02	−27	.007
TbTh (mm)	0.28 ± 0.04	0.31 ± 0.03	−10	.1
TbN (mm^{-3})	1.15 ± 0.20	1.43 ± 0.13	−20	.008
TbSp (mm)	0.62 ± 0.20	0.40 ± 0.04	55	.02
Stiffness (kN/mm)	284.77 ± 76.14	389.97 ± 84.90	−27	.04
Failure load (kN)	4.98 ± 1.23	7.01 ± 1.52	−29	.02

Note.—Unless otherwise indicated, data are means ± standard deviations.

* Percentage difference between women with AN and control subjects was calculated for trabecular parameters and mechanical parameters.

different between AN and control groups ($P < .05$). Subjects with AN had lower BV/TV and TbN and higher TbSp. TbTh was lower in women with AN ($P = .1$) (Table 2).

Finite Element Analysis

Stiffness and estimated failure load were significantly lower (−27% and −29%, respectively) in the AN group than in the control group (Table 2). Failure load was found to correlate highly with stiffness ($r = 0.99$). A plot of the von Mises stress distribution for a sample AN model is illustrated in Figure 3. The stress distribution corresponds to an axial strain of 0.34% which, for that case, corresponded to failure (ie, 2% of the bone volume exceeding 0.7% strain). The illustration highlights the high local stresses (in red on Figure 3) in the trabecular structure.

DXA Results

There were significant differences in BMD measurements at all sites between AN and control groups ($P = .001$ to $.02$) (Table 3). The percentage difference in bone density between the two groups was the greatest at the lumbar spine and femoral neck.

Correlation between DXA, Structural Parameters, and Mechanical Properties

All trabecular parameters (except TbTh) showed significant correlations with the two mechanical parameters, stiffness and failure load (Table 4). BMD measurements and *z* and T scores at the anatomic sites also demonstrated significant correlations with stiffness and failure load ($r = 0.58$ to 0.83). The strongest correlations between DXA measurements and mechanical properties were observed for BMD of the radius and the ultradistal radius. These were in the same range as correlations of BV/TV, TbN, and TbSp with the mechanical parameters. All correlations were greater for failure load than for stiffness.

Multivariate Analyses

For stepwise regression analysis, with TbN and TbTh entered into the model, TbN accounted for 57% of the variability in stiffness and failure load (Table 5). The results did not change when BV/TV was added to the model. Similarly, after controlling for body mass index, fat mass, or categorization of the groups as AN or control, TbN was an independent and positive predictor of stiffness and failure load ($P = .002$ for both). In a stepwise regression model with the same parameters entered into the model one at a time, TbN accounted for 57% of the variability of both stiffness and failure load.

Discussion

Decreased bone mass and increased risk of fracture has been demonstrated in AN (21–23). In a previous study (8), abnormal bone structure in adolescents with AN was demonstrated by using flat-panel volume CT. In the current study, we calculated mechanical properties (failure load and stiffness) by using finite element analysis on models created by using flat-panel volume CT images of the distal radius in addition to trabecular structure analysis and BMD measurements in adult women with AN and healthy control subjects of comparable age. Our data indicated significant reductions in stiffness and failure load, BMD, BV/TV, and TbN, as well as a significant increase in TbSp in the AN group. Although TbTh was also reduced in the AN group, the result was not statistically significant.

Recently, Boutroy et al (24), using high-resolution peripheral quantitative CT with a spatial resolution of 82 μm, compared volumetric bone density, trabecular structure measurements, and mechanical properties at the radius between postmenopausal women with a history of osteoporotic wrist fractures and age-matched control subjects

without a history of such fractures. Significant reductions in stiffness and strength were found between the two groups. While the isotropic resolution of 150 μm available from flat-panel volume CT is not as high as that from high-resolution peripheral quantitative CT, our images showed that flat-panel volume CT is sufficient for the visualization of the trabecular network at the distal radius (Fig 1). It is possible that some of the finer trabeculae were not included in the model; however, Pistoia et al (25) demonstrated that the results of finite element models created from micro-CT (22 μm) correlated strongly with those obtained from models based on 165-μm images by using three-dimensional peripheral quantitative CT. Our results support this finding and demonstrate that images from flat-panel volume CT can be used to create finite element models capable of distinguishing healthy from diseased bone.

In our study, we simulated an axial compression test on an axial section of the distal radius. The failure criteria we used were proposed and validated by Pistoia et al (9) and have been demonstrated to differentiate between the distal radius in healthy and osteoporotic subjects (24). A recent study by MacNeil and Boyd (12) showed that linear finite element analysis can be used to determine bone strength with a strong linear relation between stiffness and strength. Thus, linear finite element analysis is a useful approach when comparing relative bone strengths. Our strong correlation between stiffness and failure load is thus not unexpected and explains the similar correlations with the morphologic parameters and DXA measurements.

The fact that our analysis was limited to a 5-mm section is likely the reason for the higher stiffness and failure load values we obtained compared with previous studies. Other reasons for our calculated higher values may have been the choice of the threshold level for the bone segmentation (results of finite element analysis models are highly sensitive to this value [26]), the higher value used for the Young modulus, or the use of tetrahedral versus brick elements for the finite element mesh. However, while these factors would result in different absolute values for the stiffness and failure load, when comparing with previous studies, our method suffices for comparing relative bone mechanical properties between the two cohorts in this study.

Table 3

BMD Parameters Measured with DXA in AN and Control Groups

Variable	AN Group ($n = 8$)	Control Group ($n = 6$)	Percentage Difference*	*P* Value
Ultradistal radius				
BMD (g/cm^2)	0.41 ± 0.03	0.52 ± 0.06	−21	.004
z Score	−0.51 ± 0.50	1.33 ± 1.01	…	.005
T score	−0.58 ± 0.58	1.28 ± 1.02	…	.004
Distal radius				.02
BMD (g/cm^2)	0.55 ± 0.02	0.62 ± 0.05	−11	.02
z Score	−0.38 ± 0.38	0.90 ± 0.90	…	.02
T score	−0.48 ± 0.44	0.83 ± 0.92	…	
Anteroposterior lumbar spine				.001
BMD (g/cm^2)	0.84 ± 0.11	1.13 ± 0.11	−26	.006
z Score	−1.78 ± 1.01	0.33 ± 1.21	…	.001
T score	−1.91 ± 0.99	0.52 ± 0.99	…	
Lateral lumbar spine				
BMD (g/cm^2)	0.66 ± 0.09	0.85 ± 0.11	−22	.007
z Score	−1.74 ± 1.08	0.55 ± 1.42	…	.001
T score	−1.90 ± 1.07	0.38 ± 1.36	…	.008
Hip				
BMD (g/cm^2)	0.82 ± 0.14	1.10 ± 0.17	−25	.007
z Score	−1.00 ± 1.11	1.02 ± 1.25	…	.01
T score	−1.04 ± 1.15	1.32 ± 1.37	…	.007
Femoral neck				
BMD (g/cm^2)	0.72 ± 0.13	1.01 ± 0.2	−29	.01
z Score	−1.13 ± 1.10	1.02 ± 1.35	…	.01
T score	−1.20 ± 1.17	1.42 ± 1.74	…	.01

Note.—Unless otherwise indicated, data are means ± standard deviations.

* Percentage difference between women with AN and control subjects was calculated for the BMD variable at the anatomic sites.

Figure 3

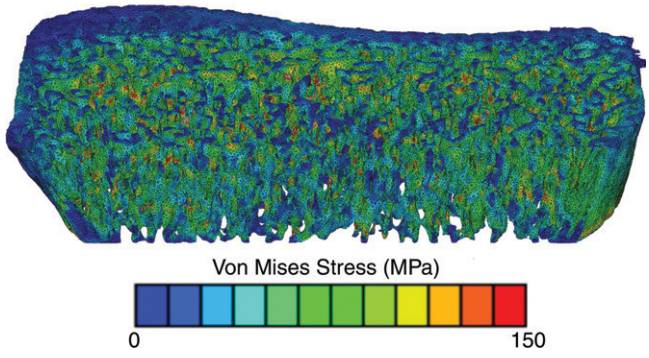

Figure 3: Colored representation of the von Mises stress distribution resulting from the finite element analysis for a woman with AN. This illustration is for 0.34% axial strain, which corresponds to simulated failure of the bone (ie, 2% of bone volume exceeding the elastic strain limit).

Table 4

Correlation between Morphologic Parameters, DXA Measurements, and Mechanical Parameters Presented as the Whole Cohort

	Stiffness		Failure Load	
Parameter	*r* Value	*P* Value	*r* Value	*P* Value
BV/TV	0.72	.004	0.74	.003
TbTh	0.44	.111	0.48	.08
TbN	0.75	.002	0.76	.002
TbSp*	−0.73	.003	−0.78	.001
Radius				
BMD	0.78	.002	0.82	.001
z Score	0.75	.003	0.80	.001
T score	0.77	.002	0.82	.001
Ultradistal radius				
BMD	0.78	.002	0.83	.0005
z Score	0.77	.002	0.82	.0005
T score	0.78	.002	0.83	.0004
Anteroposterior lumbar spine				
BMD (g/cm^2)	0.67	.093	0.71	.005
z Score	0.58	.028	0.61	.02
T score	0.67	.009	0.71	.005
Lateral lumbar spine				
BMD (g/cm^2)	0.64	.014	0.69	.006
z Score	0.60	.024	0.65	.01
T score	0.64	.014	0.69	.007
Hip				
BMD (g/cm^2)	0.70	.005	0.76	.002
z Score	0.65	.011	0.70	.005
T score	0.70	.005	0.75	.002
Femoral neck				
BMD (g/cm^2)	0.74	.003	0.79	.001
z Score	0.71	.005	0.76	.002
T score	0.73	.003	0.78	.001

* The nonparametric Spearman rho test was used for TbSp, because this parameter is not normally distributed.

Table 5

Regression Model with Radius TbN

Mechanical Parameter	Parameter Estimate	F Ratio	*P* Value	R^2
Failure load				
Intercept	−1.404	…	…	…
TbN	5.701	16.1	.002	0.57
Stiffness				
Intercept	−75.86	…	…	…
TbN	318.67	15.7	.002	0.57

Our data demonstrated significant correlations between all BMD measurements and trabecular structure measurements (except TbTh) and stiffness and failure load. The strongest correlations with stiffness and strength were for the ultradistal radius followed by the radius. The inclusion of the cortical shell in the measurements of BMD is a possible reason that these correlations with mechanical parameters were slightly higher than those observed for the trabecular architectural indexes. Previous studies have shown that a high percentage of the load is borne by the distal cortex (24). The lack of a significant correlation with TbTh has previously been found by Pistoia et al (9) where a similar resolution was used (165 μm). This may be due to the exclusion of smaller trabeculae because of limitations in spatial resolution. MacNeil and Boyd (12) compared trabecular structure measurements obtained from human radius specimens (age range, 55–93 years) by using high-resolution peripheral quantitative CT (82 μm) with those obtained by using micro-CT (19 μm) and found that TbTh was most affected by the reduced resolution.

The primary site of interest in this study was the distal radius, although BMD measurements were also obtained for the femoral neck, hip, and spine. The advantage of analyzing trabecular structure and mechanical properties of the distal radius is that its peripheral location allows CT images to be obtained quickly and without direct or indirect exposure of reproductive organs in our young population. Furthermore, structure parameters of the distal radius had been proved to be valuable in prediction of vertebral fractures (27).

There were several limitations to this study. First, the number of patients with AN and control subjects included in this study was relatively small; a larger study would allow to adjust for multiple comparison analysis. However, even with this small data set, all parameters except TbTh showed significant differences between the two groups. Second, simplified models and boundary conditions used for finite element analysis meant that it was not possible to simulate perfectly physiologic loading conditions. However, while this method does not realistically simulate the boundary conditions during a fall, it has been well correlated to mechanical testing (9). Third, the weakest point of bone or potential fracture site may lie outside of the examined region and thus may not represent actual failure load. Fourth, we only assessed structure and mechanical properties of trabecular bone. Further studies evaluating the role of cortical bone are needed. Finally, because this study was cross-sectional in nature, the lack of follow-up did not allow true fracture risk to be confirmed. However, on the basis of similar degradation in cortical and trabecular bone found in studies in osteoporotic patients with a history of fractures (7), our data suggest that altered bone microarchitecture in these women with AN may also indicate an increased risk of fractures.

In conclusion, we have shown reduced calculated stiffness and failure

load of the distal radius in women with AN compared with age-matched healthy control subjects by using finite element models created from 150-μm resolution flat-panel volume CT; reductions in BV/TV, TbN, and BMD and an increase in TbSp were observed in the AN group.

Acknowledgments: The authors thank the staff at Materialise for providing the MIMICS software for creating the three-dimensional finite element models based on flat-panel volume CT images and for their generous guidance on creating the three-dimensional models. We acknowledge the guidance of Tomasz Wierzbicki, PhD, from the Massachusetts Institute of Technology during the early stages of this project and the use of his Abaqus software.

References

1. Pope HG, Hudson JI, Yurgelun-Todd D, Hudson MS. Prevalence of anorexia nervosa and bulimia in three student populations. Int J Eat Disord 1984;3(3):45–51.
2. Lucas AR, Beard CM, O'Fallon WM, Kurland LT. 50-year trends in the incidence of anorexia nervosa in Rochester, Minn.: a population-based study. Am J Psychiatry 1991;148(7):917–922.
3. Biller BM, Saxe V, Herzog DB, Rosenthal DI, Holzman S, Klibanski A. Mechanisms of osteoporosis in adult and adolescent women with anorexia nervosa. J Clin Endocrinol Metab 1989;68(3):548–554.
4. Rigotti NA, Nussbaum SR, Herzog DB, Neer RM. Osteoporosis in women with anorexia nervosa. N Engl J Med 1984;311(25):1601–1606.
5. Grinspoon S, Thomas E, Pitts S, et al. Prevalence and predictive factors for regional osteopenia in women with anorexia nervosa. Ann Intern Med 2000;133(10):790–794.
6. Keaveny TM, Morgan EF, Niebur GL, Yeh OC. Biomechanics of trabecular bone. Annu Rev Biomed Eng 2001;3:307–333.
7. Boutroy S, Bouxsein ML, Munoz F, Delmas PD. In vivo assessment of trabecular bone microarchitecture by high-resolution peripheral quantitative computed tomography. J Clin Endocrinol Metab 2005;90(12):6508–6515.
8. Bredella MA, Misra M, Miller KK, et al. Distal radius in adolescent girls with anorexia nervosa: trabecular structure analysis with high-resolution flat-panel volume CT. Radiology 2008;249(3):938–946.
9. Pistoia W, van Rietbergen B, Lochmüller EM, Lill CA, Eckstein F, Rüegsegger P. Estimation of distal radius failure load with micro-finite element analysis models based on three-dimensional peripheral quantitative computed tomography images. Bone 2002;30(6):842–848.
10. Pistoia W, van Rietbergen B, Lochmüller EM, Lill CA, Eckstein F, Rüegsegger P. Image-based micro-finite-element modeling for improved distal radius strength diagnosis: moving from bench to bedside. J Clin Densitom 2004;7(2):153–160.
11. Ulrich D, van Rietbergen B, Laib A, Rüegsegger P. Load transfer analysis of the distal radius from in-vivo high-resolution CT-imaging. J Biomech 1999;32(8):821–828.
12. MacNeil JA, Boyd SK. Bone strength at the distal radius can be estimated from high-resolution peripheral quantitative computed tomography and the finite element method. Bone 2008;42(6):1203–1213.
13. Gupta R, Grasruck M, Suess C, et al. Ultra-high resolution flat-panel volume CT: fundamental principles, design architecture, and system characterization. Eur Radiol 2006;16(6):1191–1205.
14. American Psychiatric Association. Diagnostic and statistical manual of mental disorders. Washington, DC: American Psychiatric Association, 2000.
15. Botolin S, Faugere M-C, Malluche H, Orth M, Meyer R, McCabe LR. Increased bone adiposity and peroxisomal proliferator-activated receptor-gamma2 expression in type I diabetic mice. Endocrinology 2005;146(8):3622–3631.
16. Sheng ZF, Dai RC, Wu XP, Fang LN, Fan HJ, Liao EY. Regionally specific compensation for bone loss in the tibial trabeculae of estrogen-deficient rats. Acta Radiol 2007;48(5):531–539.
17. Liu SP, Liao EY, Chen J, et al. Effects of methylprednisolone on bone mineral density and microarchitecture of trabecular bones in rats with administration time and assessed by micro-computed tomography. Acta Radiol 2009;50(1):93–100.
18. Otsu N. A threshold selection method from gray-level histograms. IEEE Trans Syst Man Cybern 1979;9(1):62–66.
19. Parfitt AM. Bone histomorphometry: proposed system for standardization of nomenclature, symbols, and units. Calcif Tissue Int 1988;42(5):284–286.
20. Kaplan FS, Hayes WC, Keaveny TM, Boskey A, Einhorn TA, Iannotti JP. Form and function of bone. In: Simon SR, ed. Orthopaedic basic science. Rosemont, Ill: American Academy of Orthopaedic Surgeons, 1994;127–184.
21. Milos G, Spindler A, Rüegsegger P, et al. Cortical and trabecular bone density and structure in anorexia nervosa. Osteoporos Int 2005;16(7):783–790.
22. Milos G, Spindler A, Rüegsegger P, et al. Does weight gain induce cortical and trabecular bone regain in anorexia nervosa? a two-year prospective study. Bone 2007;41(5):869–874.
23. Galusca B, Zouch M, Germain N, et al. Constitutional thinness: unusual human phenotype of low bone quality. J Clin Endocrinol Metab 2008;93(1):110–117.
24. Boutroy S, Van Rietbergen B, Sornay-Rendu E, Munoz F, Bouxsein ML, Delmas PD. Finite element analysis based on in vivo HR-pQCT images of the distal radius is associated with wrist fracture in postmenopausal women. J Bone Miner Res 2008;23(3):392–399.
25. Pistoia W, van Rietbergen B, Laib A, Rüegsegger P. High-resolution three-dimensional-pQCT images can be an adequate basis for in-vivo microFE analysis of bone. J Biomech Eng 2001;123(2):176–183.
26. Kim CH, Zhang H, Mikhail G, et al. Effects of thresholding techniques on microCT-based finite element models of trabecular bone. J Biomech Eng 2007;129(4):481–486.
27. Link TM, Bauer J, Kollstedt A, et al. Trabecular bone structure of the distal radius, the calcaneus, and the spine: which site predicts fracture status of the spine best? Invest Radiol 2004;39(8):487–497.